JCTC Journal of Chemical Theory and Computation

A Fourier Transform Method for Generation of Anharmonic Vibrational Molecular Spectra

Ivan Ivani,[‡] Vladimír Baumruk,[‡] and Petr Bouř*,[†]

Institute of Organic Chemistry and Biochemistry, Academy of Sciences, 166 10 Prague, Czech Republic, and Charles University, Faculty of Mathematics and Physics, Institute of Physics, Ke Karlovu 5, 12116, Prague, Czech Republic

Received March 18, 2010

Abstract: Accurate computations of vibrational energies and vibrational spectra of molecules require inclusion of the anharmonic forces. In standard computational protocols, this leads to a large vibrational Hamiltonian matrix that needs to be diagonalized. Spectral intensities are calculated for individual transitions separately. In this work, an alternate direct generation of the spectral curves is proposed, based on a temporal propagation of a trial vibrational wave function followed by the Fourier transformation (FT). The method was applied to model water dimer and fenchone molecules. Arbitrary resolutions could be achieved by longer-time propagations, although a smaller integration time step (∼0.02 fs) was needed for accurate peak frequencies than previously found for similar time-dependent applications within the harmonic approximation. Acceptably accurate relative vibrational spectra intensities were obtained when many random vectors used in the propagations were averaged. For a model fenchone Hamiltonian, simulated Raman and Raman optical activity (ROA) spectral shapes compared well with those obtained by the classical approach. The algorithm is amendable to parallelization. The lack of the lengthy and computer-memory-demanding diagonalization thus makes the FT procedure especially convenient for spectral simulations of larger molecules.

I. Introduction

Simulations of vibrational spectra are necessary to understand experimental data, and to obtain extensive information about molecular structures and force fields. Particularly for peptides, nucleic acids, and other biologically relevant systems, the vibrational spectroscopy provides a valuable means for the monitoring of specific structural and conformational features.[1] Historically, first spectral analyses were carried out by empirical correlations of IR or Raman band frequencies with the geometry.[2] Later theoretical approaches were based on simplified vibrational calculations, e.g., through parametrized force fields (FFs).[3] Today, precise and fast quantum mechanical computations[4] provide the most flexible way for theoretical spectral analyses. In particular, the density functional theory approximations can be applied for larger molecules, including intensity simulations for experiments with unpolarized as well as, for example, circularly polarized radiation.[5]

The harmonic approximation based on the second derivatives of the nuclear potential[6] is sufficient for many applications. Any molecule behaves like a system of independent harmonic oscillators at the harmonic limit. Typically, spectra of large biopolymers (nucleic acids, peptides) are simulated with this assumption because of the low resolution, limited spectral range, inhomogeneous band broadening caused by the solvent and molecular dynamics, and limited precision of available force fields.[1] For better accuracy or more advanced applications, anharmonic potential parts need to be included.[7−10] Beyond the harmonic model, computation of molecular vibrational energies is no more a black box method, but advanced computational schemes are needed, including vibrational configuration interaction (VCI),[11−13] vibrational self-consistent field (VSCF),[9,14−16] many-body perturbation theory (PT),[17,18] vibrational coupled clusters,[19] etc.

* Corresponding author e-mail: bour@uochb.cas.cz.
[†] Academy of Sciences.
[‡] Charles University.

10.1021/ct100150f
Published on Web 06/28/2010

The VCI scheme, where the wave function is expressed as a linear combination of harmonic oscillator functions, is probably the most universal and most straightforward procedure. Unlike for the VSCF and PT approaches, fundamental and combination energy levels and spectral transitions can be obtained at the same time. Although VCI may become impractical for large systems,[18,20] it represents an important benchmark as it is, in principle, equivalent to the exact Schrödinger solution. Unfortunately, similarly as for the electronic configuration interaction (CI),[21] the dimension of the Hamiltonian required for a reasonable result quickly grows with the size of the molecule. Unlike for the electronic problem, however, where only few lowest-energy states are usually needed, a large portion of the vibrational energy levels covering the spectrum is required for vibrations.

Thus, a complete diagonalization of the vibrational Hamiltonian is typically needed to provide the transition energies, corresponding peak positions, and wave functions (eigenvectors) bearing spectral intensities. The classical in-memory iteration diagonalization routines are most convenient for small and medium dimensions ($N < \sim 10^4$).[22,23] These direct algorithms occupy computer memory that is approximately proportional to N^2 and require times that scale as N^3. Larger matrices can be more conveniently diagonalized, at least partially, by so-called power iteration methods, often referred to as (Jacobi-)Davidson algorithms, which perform the actual diagonalization in an intermediate (Krylov) vector space.[24−28] The actual eigenspace can be built from the largest or from the smallest eigenvalue. The matrix does not need to be stored in memory, and the algorithm is simple, requiring essentially many matrix−vector multiplications only. When the matrix is sparse (which is often the case with the harmonic oscillator basis and a polynomial anharmonic potential), multiplications by the zeros can easily be avoided.

As each vector has to be orthonormalized against the previous ones, however, complete Davidson diagonalizations become difficult for larger matrices. It is also important to point out that for many applications detailed eigenvalue information is not needed. In particular for condensed phase spectroscopy, calculated line intensities are often convoluted with Gaussian or Lorentzian bands of finite widths, to simulate the inhomogeneous line broadening present in the experiment. Already for medium-sized molecules, observable peaks are usually composed from many unresolved vibrational transitions. Line spectrum simulations thus appear superfluous, whereas it is the spectral envelope that is desirable for comparison with the experiment to relate the structure and spectral response.

Therefore, the Fourier methods (Figure 1) may be a better option for unresolved spectral shapes. Within the harmonic limit, for example, it can be shown that classical molecular dynamic trajectories provided exact quantum results.[29] Propagation of a fictitious wave function in an arbitrary time was previously proposed to diagonalize giant Hessians and to generate corresponding vibrational spectra instead.[30] For large molecules, the Fourier transformation was much faster than the conventional diagonalizations. The spectral profiles were obtained by propagation and averaging of many trial vectors. However, the methods required the harmonic shape

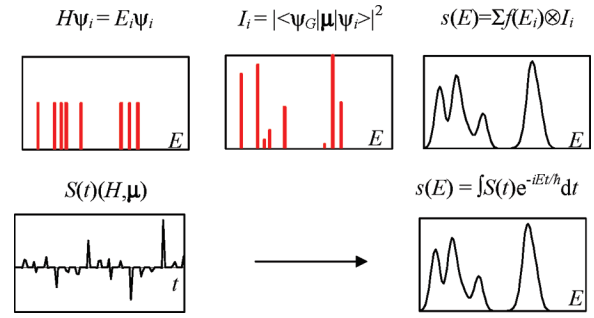

Figure 1. Schematic representation of the two processes of simulating vibrational spectra: (Top) By the usual way, discrete energies are found by a Hamiltonian (H) diagonalization; the intensities (I) are calculated from the eigenfunctions ψ and, for example, dipole moment μ, and the spectrum $s(E)$ is created by a convolution with an arbitrary peak shape f. (Bottom) Within the Fourier method, spectral function (S) develops in time, and the transformation provides the spectrum directly.

of the nuclear potential. In this work, we propose and test a different scheme suitable for a general anharmonic problem.

Time-dependent methods have always been popular in computational chemistry and were applied, for example, to simulations of the nuclear magnetic resonance,[31] Raman scattering, infrared absorption, and vibrational circular dichroism.[32,33] Anharmonic vibrational systems were also investigated; however, it should be noted that previous methods based on integration of classical trajectories do not provide all anharmonic corrections, such as the intermode coupling.[32,34,35]

Modern mechanics−molecular mechanics (QM/MM) methods also facilitate computation of the spectra via time-dependent properties.[36,37] In particular, more advanced spectroscopic experiments, such as the vibrational circular dichroism (VCD) or the two-dimensional (2D) spectroscopy, profit from various Fourier techniques.[38−42] As a special class, the time-dependent filter-diagonalization methods[22] make the spectral generation more efficient for a preselected frequency interval.[43] The methods are based on both classical[44−46] and ab initio molecular dynamics trajectories[47−49] but are mostly restricted to the harmonic potential.[29]

Similarly, in the electronic spectroscopy and reactions, schemes like the multiconfigurational time-dependent Hartree approach[50] facilitate dynamic calculations for polyatomic molecules, a topic which goes beyond the scope of the present study. Rather than model real time-dependent processes, we introduce the time-dependent wave function and a spectral (e.g., dipole) function with the sole purpose of obtaining exact anharmonic energies and relative spectral intensities (including special polarized spectroscopies) for a general vibrational Hamiltonian. As the transition energies are needed rather than vibrational state energies, the exact ground state is obtained before the temporal propagation by the Davidson method. This, however, does not significantly increase the computational effort, unlike a complete Davidson diagonalization.

II. Theory

Consider a Hamiltonian H, wave functions $|K\rangle$, and energies E_K obliging the Schrödinger equation, $H|K\rangle = E_K|K\rangle$. A

general time-dependent wave function can be written as a sum, $\psi(t) = \sum_{K=1,N} d_K|K\rangle \exp(-iE_Kt/\hbar)$, and propagated according to the time-dependent Schrödinger equation, $i\hbar\dot{\psi}(t) = H\psi(t)$, where $\hbar$ is the Planck constant, d_K represents expansion coefficients, and N is the number of the basis functions. In the discrete time integration scheme detailed below, we calculated the wave function at time $t + dt$ as

$$\psi(t + dt) \cong \psi(t) + \dot{\psi}(t)dt + \frac{1}{2}\ddot{\psi}(t)dt^2 \quad (1)$$

with $\dot{\psi}(t) = H/(i\hbar)\ \psi(t)$, and $\ddot{\psi}(t)\ dt^2 = \psi(t) + \psi(t - 2dt) - 2\psi(t - dt)$; the wave function was renormalized at each time step.

The vibrational ground state $|G\rangle$ can easily be obtained by the Davidson diagonalization,[25,51] as the first eigenvector. As pointed out in the Introduction, because the diagonalization becomes very inefficient for a large amount of required vectors,[30,51] temporal propagations will be used to obtain spectral intensities coming from the remaining states instead.

The ground state wave function, besides the numerical propagation (eq 1), can also be propagated analytically as $\psi_G(t) = |G\rangle \exp(-iE_Gt/\hbar)$, where E_G is the ground state energy. Additionally, we propagate a random function R and, for example, a dipole integral for the absorption spectrum

$$\boldsymbol{\mu}_R(t) = \langle R^*(t)|\hat{\boldsymbol{\mu}}|\psi_G(t)\rangle \quad (2)$$

where $\hat{\boldsymbol{\mu}}$ is the dipole moment operator. Adaptations for other spectral types are described below. The vector can always be thought of as decomposed to the exact solutions, $R(0) = \sum_K d_K^R\psi_K(0)$, where d_K^R represents unknown coefficients, so that

$$\boldsymbol{\mu}_R(t) = \sum_K d_K^{R*}\langle K|\hat{\boldsymbol{\mu}}|G\rangle\ \mathrm{e}^{i\omega_{KG}t} \quad (3)$$

$\omega_{KG} = (E_K - E_G)/\hbar$, which can be Fourier-transformed to

$$\boldsymbol{\mu}_R(\omega) = \int \boldsymbol{\mu}_R(t)\ \mathrm{e}^{-i\omega t}\ dt = 2\pi\sum_K d_K^{R*}\langle K|\hat{\boldsymbol{\mu}}|G\rangle\delta(\omega_{KG} - \omega) \quad (4)$$

Next, we define the absorption spectrum as

$$I_R(\omega) = \frac{\sqrt{2\pi}dN\omega}{4\pi^2}\left|\boldsymbol{\mu}_R(\omega)\right|^2 = \sum_K \langle K|\hat{\boldsymbol{\mu}}|G\rangle \cdot \langle G|\hat{\boldsymbol{\mu}}|K\rangle\omega\delta(\omega_{KG} - \omega) \quad (5)$$

In the derivation of eq 5 from 4, we used $\delta(\omega_{KG'} - \omega)\delta(\omega_{K'G'} - \omega) \approx 1/(d\sqrt{2\pi})\delta_{KK'}\delta(\omega_{K'G'} - \omega)$, which is valid for approximate "δ functions" in a form of Gaussian bands, with a bandwidth d, $\delta_d(\omega) \approx \exp(-\omega^2/d^2)/(d\sqrt{\pi})$.

In order to remove the dependence on the choice of the initial vector R, the unknown state weights were replaced by the average, $|d_K^R|^2 \approx 1/N$. Note, that although the averaging was realized for expanding the vector to the harmonic oscillator basis, $R(0) = \sum_i r_i\varphi_i$, average expansion coefficients for any other orthogonal basis (in this case, the states ψ_K) are the same: Indeed, as the two $\{\varphi_i\}$ and $\{\psi_i\}$ sets are complete, we can always write $r_i = \sum_J d_J^R U_{iJ}$, where $\mathbf{U}$ is a unitary transformation (rotation) matrix. For uncorrelated random numbers d_J^R within the interval $(-1,1)$, we obtain $\langle d_J^R d_I^R\rangle = \langle d_J^{R2}\rangle\delta_{IJ}$, so that $\langle r_i^2\rangle = \langle d_J^{R2}\rangle$. In other words, the averaging in any basis set provides the same final distribution.

Many random functions R_m ($m = 1-M$) were propagated to average the resultant intensities. Then, if the absorption index is defined as

$$\varepsilon(\omega) = (9.184 \times 10^{-3}M)^{-1}\sum_{R=1,M} I_R(\omega) \quad (6)$$

the dipole strength of each resolved transition $G \rightarrow K$ is equal to the usual relation[52] $D_{KG} = 9.184 \times 10^{-3}\int \varepsilon\ \mathrm{d}\omega/\omega$, where $D_{KG} = \langle K|\hat{\boldsymbol{\mu}}|G\rangle\cdot\langle G|\hat{\boldsymbol{\mu}}|K\rangle$ is in debye^2 and ε is in L mol^{-1} cm^{-1}. In practical simulations, however, we used scaling of the calculated intensities by an empirical factor, based on a comparison of integrated IR and Raman intensities (calibrated for the water dimer). This procedure would eliminate the deviation of the simulated bands from ideal Gaussian functions. It should also be noted that exact absolute intensity simulations are not needed in most applications, as the relative band intensities bear most of the structural information.

The model vibrational Hamiltonian was chosen as

$$H = \frac{1}{2}\sum_{i=1}^{3n}(P_i^2 + \omega_i^2Q_i^2) + \frac{1}{6}\sum_{i=1}^{3n}\sum_{j=1}^{3n}\sum_{k=1}^{3n}c_{ijk}Q_iQ_jQ_k + \frac{1}{24}\sum_{i=1}^{3n}\sum_{j=1}^{3n}\sum_{k=1}^{3n}\sum_{l=1}^{3n}d_{ijkl}Q_iQ_jQ_kQ_l \quad (7)$$

where $P_i = -i\hbar\partial/Q_i$, Q_i is normal mode coordinate, ω_i is the fundamental frequency, and n is the number of atoms. All cubic (c_{ijk}) and semidiagonal quartic (d_{jjkl} etc.; at least two indices were the same) constants were included. The size of the Hamiltonian was controlled by skipping the lowest-frequency modes and by considering harmonic states φ_i that significantly interact with the ground or fundamental (F) vibrations ($|\langle\varphi_i|V|F\rangle/(E_i - E_F)| \geq$ threshold, where V represents the two last sums in eq 7). The threshold was set to 0 for the water dimer (all $0-5\times$ excited states included), and to 0.01 by default for the fenchone molecule. For the dimer, all modes were included, while for fenchone the six lowest modes were ignored. Only nonzero elements of $\mathbf{H}$ were stored in memory.

III. Implementation

The algorithm derived above was implemented within the S4[53] Fortran code as follows:

(1) Calculate the Cartesian dipole derivatives $\boldsymbol{\mu}_\mathbf{R} = \partial\boldsymbol{\mu}/\partial\mathbf{R}$; if required, calculate also the second dipole derivatives $\boldsymbol{\mu}_{\mathbf{RR}} = \partial^2\boldsymbol{\mu}/(\partial\mathbf{R}\partial\mathbf{R})$, by a numerical differentiation. The Gaussian[54] program was used for the ab initio computations.

(2) Transform the first (second) derivatives into the normal mode coordinates, using the Cartesian-normal mode transformation ($3n \times 3n$) matrix $\mathbf{S}$, $\boldsymbol{\mu}_\mathrm{Q} = \mathbf{S}\cdot\boldsymbol{\mu}_\mathbf{R}$ ($\boldsymbol{\mu}_{\mathbf{QQ}} = \mathbf{S}^t\cdot\boldsymbol{\mu}_{\mathbf{RR}}\cdot\mathbf{S}$).

(3) Construct the vibrational Hamiltonian matrix $\mathbf{H}$ in the $N \times N$ harmonic oscillator basis $\{\varphi_i\}$, $i = 1-N$.

(4) Calculate the ground eigenvector $\mathbf{g}$ ($|G\rangle = \sum_i g_i|\varphi_i\rangle$) fulfilling $\mathbf{H}\cdot\mathbf{g} = E_G\mathbf{g}$, by the Davidson iteration.

(5) Precalculate the dipole matrix $\mathbf{u}$, $\mathbf{u}_i(0) = \sum_j g_j\langle\varphi_j|\hat{\boldsymbol{\mu}}|\varphi_i\rangle$,

where $\hat{\boldsymbol{\mu}} = \sum_{i=1}^{3n}\boldsymbol{\mu}_{Q_i}Q_i + {}^1/_2\sum_{i=1}^{3n}\sum_{j=1}^{3n}\boldsymbol{\mu}_{Q_iQ_j}Q_iQ_j$ is the vibrational dipole.

(6) Initialize the complex dipole function in the frequency domain (on a grid, typically 2000 points within 0−4000 cm^{-1}), $\boldsymbol{\mu}(\omega) = 0$, set time $t = 0$, and iteration step $k = 0$. In a set of complex random vectors $\mathbf{r}_m$ ($m = 1-M$), set each component $r_{m,i}$ ($i = 1-N$) to a random number within (−1 to +1) and normalize, so that $|\mathbf{r}_m| = 1$.

(7) Increment time t by dt and obtain:

New vectors $\mathbf{r}_m^{(k+1)} = \mathbf{r}_m^{(k)} - (i/\hbar)\mathbf{H}\cdot\mathbf{r}_m^{(k)} + {}^1/_2\mathbf{d}2_m^{(k)}$.

Updated second derivatives $\mathbf{d}2_m^{(k+1)} = (\mathbf{r}_m^{(k)} + \mathbf{r}_m^{(k-2)} - 2\mathbf{r}_m^{(k-1)})/dt$.

Dipoles $\boldsymbol{\mu}_m(t) = \mathbf{r}_m\cdot\mathbf{u}\exp(-iE_Gt/\hbar)$. The scalar products in step 7 are related to the HO index, spanning $1-N$.

(8) Accumulate the dipole spectrum $\boldsymbol{\mu}(\omega) = \boldsymbol{\mu}(\omega) + e^{-i\omega t}\boldsymbol{\mu}_m(t)dt$, for each m.

(9) If $k < k_{max}$, goto 7.

(10) From $\boldsymbol{\mu}(\omega)$, calculate the intensity according to eqs 5 and 6.

Modifications for Other Spectral Types. The algorithm above was derived for infrared absorption intensities. For vibrational circular dichroism (VCD), in steps 1 and 2, we additionally need to calculate Cartesian ($\mathbf{m}_C = \partial\mathbf{m}/\partial\mathbf{p}$, atomic axial tensor, AAT) and, consequently, normal mode ($\mathbf{m}_Q = \partial\mathbf{m}/\partial\mathbf{P}$) derivatives of the magnetic dipole moment $\mathbf{m}$,[55] where $\mathbf{p}$ and $\mathbf{P}$ are the respective nuclear and normal mode momenta. The second-order anharmonic contribution was neglected for VCD and other spectral types. In step 5, besides matrix $\mathbf{u}$, we calculate $\mathbf{m}_i(0) = \sum_j g_j\langle\varphi_j|\mathbf{m}|\varphi_i\rangle$, where $\mathbf{m} = \mathbf{m}_Q\cdot\mathbf{P}$ is the vibrational magnetic dipole. The dipoles $\mathbf{m}_m(t) = \mathbf{r}_m\cdot\mathbf{m}\exp(-iE_Gt/\hbar)$ are propagated in steps 6−9 for each random vector, and a frequency function $\mathbf{m}_m(\omega)$ is obtained in analogy to the electric dipole. The VCD spectrum corresponding to each m vector is $I_m(\omega) = [\sqrt{(2\pi)}dN\omega]/[4\pi^2]\,\mathrm{Im}(\boldsymbol{\mu}_m^*(\omega)\cdot\mathbf{m}_m(\omega))$.

Raman spectra for various experimental setups can be obtained in a similar way, by replacing the dipole operator $\hat{\boldsymbol{\mu}} = \sum_{i=1}^{3n}\boldsymbol{\mu}_{Q_i}Q_i + {}^1/_2\sum_{i=1}^{3n}\sum_{j=1}^{3n}\boldsymbol{\mu}_{Q_iQ_j}Q_iQ_j$ by electric polarizability, $\hat{\boldsymbol{\alpha}} = \boldsymbol{\alpha}_Q\cdot\mathbf{Q} + {}^1/_2\mathbf{Q}\cdot\boldsymbol{\alpha}_{QQ}\cdot\mathbf{Q}$. For backscattering Raman intensity,[55,56] for example, we get $I_{R,180}(\omega) = K/(1 - \exp(-\omega/kT))\sum_{\alpha=1-3}\sum_{\beta=1-3}\mathrm{Re}(7\boldsymbol{\alpha}_{R,\alpha\beta}^*(\omega)\boldsymbol{\alpha}_{R,\alpha\beta}(\omega) + \boldsymbol{\alpha}_{R,\alpha\alpha}(\omega)^*\boldsymbol{\alpha}_{R,\beta\beta}(\omega))$. The constant K was chosen to be 1 (note that absolute intensities are rarely measured); k is the Boltzmann constant and T the temperature. The exponential factor accounts for scattering from excited vibrational levels as derived in the harmonic limit.[56] An alternative more exact path, based on individual low-energy states, used instead of the ground state and transitions weighed by the Boltzmann population, was not attempted. In that case, the temperature factor would have been omitted. However, anharmonic spectral correction in the lowest-wavenumber region, most affected by the temperature, is for most molecules rather small, and the harmonic-like temperature correction is thus sufficient.

By replacing the dipole operator by the electric dipole−magnetic dipole polarizability, $\hat{\mathbf{G}}' = \mathbf{G}'_Q\cdot\mathbf{Q} + {}^1/_2\mathbf{Q}\cdot\mathbf{G}'_{QQ}\cdot\mathbf{Q}$ (also referred to as the optical rotation tensor), and the electric dipole−electric quadrupole polarizability, $\hat{\mathbf{A}} = \mathbf{A}_Q\cdot\mathbf{Q} + {}^1/_2\mathbf{Q}\cdot\mathbf{A}_{QQ}\cdot\mathbf{Q}$, we can calculate Raman optical activity. The backscattering incident circular polarized light intensity[55] was obtained as

$$\Delta I_{R,180}(\omega) = \frac{8K}{1-\exp(-\omega/kT)}\sum_{\alpha=1-3}\sum_{\beta=1-3}\mathrm{Re}(3\boldsymbol{\alpha}_{R,\alpha\beta}^*(\omega)\mathbf{G}'_{R,\alpha\beta}(\omega) - \boldsymbol{\alpha}_{R,\alpha\alpha}^*(\omega)\mathbf{G}'_{R,\beta\beta}(\omega) + \sum_{\delta=1-3}\sum_{\gamma=1-3}\varepsilon_{\alpha\gamma\delta}\boldsymbol{\alpha}_{R,\alpha\beta}(\omega)^*\mathbf{A}_{R,\gamma\delta\beta}(\omega))$$

The B3LYP[57]/6311++G** method was used to compute the energy derivatives and the intensity tensors, as implemented in the Gaussian program.[54] Water dimer and the fenchone molecule (Figure 2) in equilibrium geometries were used for the modeling. Model VCI Hamiltonians with dimensions of 1325 (water) and 49 584 (fenchone) were used by default for most calculations; for fenchone, dimensions of 180, 509, 1456, 3560, 5689, and 119 817 were additionally used for the timing tests.

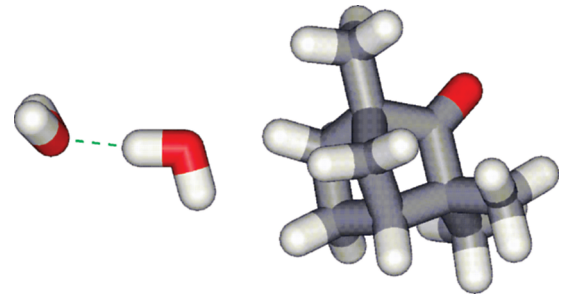

Figure 2. Water dimer and the fenchone molecule B3LYP/6-311++G** geometries.

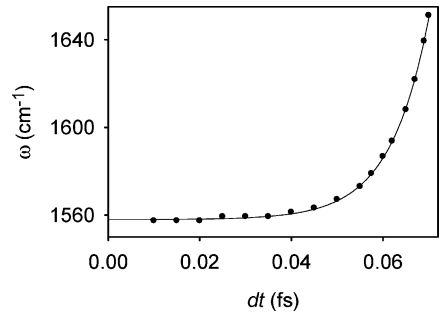

Figure 3. Dependence of the water HOH bending band frequency on the integration step, for water dimer.

IV. Results

For exact Fourier transformation, the peak positions[23,58] in the ω spectrum are constant. As was shown before already for the harmonic case,[29] in practical numerical integrations, larger time steps lead to overestimation of the peak frequencies. Indeed, as shown in Figure 3, where the water dimer bending vibration frequency is plotted as a function of the integration time step, larger steps (>0.06 fs) introduce errors of over 100 cm^{-1}. Only for steps below ~0.02 fs does the frequency stabilize. This is a relatively small fraction of the period of the corresponding harmonic motion, $T = 2\pi/\omega \approx 21$ fs. For harmonic wave function propagations, longer integration steps of ~0.1 fs could be used.[29] For some computations, however, steps as large as 2.4 fs were

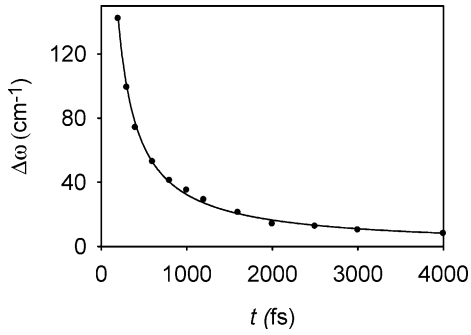

Figure 4. Dependence of the water dimer bending bandwidth on the integration time, for $dt = 0.02$ fs.

proposed.[43] We explain the need to use shorter integration steps for the anharmonic case even for lower-frequency states by a coupling to the higher-frequency states included in the Hamiltonian.

As follows from the general theory of Fourier transformation, the bandwidth is inversely proportional to the integration time, $\Delta\omega \sim t^{-1}$.[23,58] This is also observed in the calculated dependence for the water dimer in Figure 4. As the width converges relatively slowly, the method does not seem to be usable for high-resolution spectra; in that case, many spectral points are additionally needed per frequency interval, which would further slow down the computations. On the other hand, the inhomogeneous band broadening is quite large for typical biomolecular spectra, on the order of ~20 cm^{-1},[59,60] so that the propagation times can be limited. That means that for a 0.02 fs time step (used to achieve a high precision of central frequencies, cf. Figure 3), about 4000/0.2 = 200 000 propagation points are needed.

Although the spectral intensities that can be obtained with the FT method are only approximate, for a large number of the random vectors, relative band ratios are reasonably close to the exact result. This is documented in Figure 5, where backscattering Raman and ROA spectra of fenchone are simulated for M (number of the vectors) = 5, 10, and 50 and compared to exact intensities calculated by the direct diagonalization of the model 49 584 × 49 584 VCI Hamiltonian. Already for $M = 5$, the raw Raman spectral profile is similar to the direct calculation; the relative peak ratios are further improved for $M = 50$. The ROA signal converges more slowly, especially within the 1400−1600 cm^{-1} region, where many overlapped transitions (mostly C−H bending vibrations) are present. However, the simulation $M = 50$ provides the correct relative intensity and sign pattern for ROA, too. Both the Raman and ROA CH stretching higher-frequency signal seems to converge faster than that for vibrations below 2000 cm^{-1}. The calculated vibrational frequencies correspond reasonably well to the observed values;[61] however, we leave a detailed comparison to the experimental spectral profiles for a future study because of the complexity of the problem.

As a more exact means to document the convergence, in Figure 6, part A, we plot an example of an actual r_{mi}

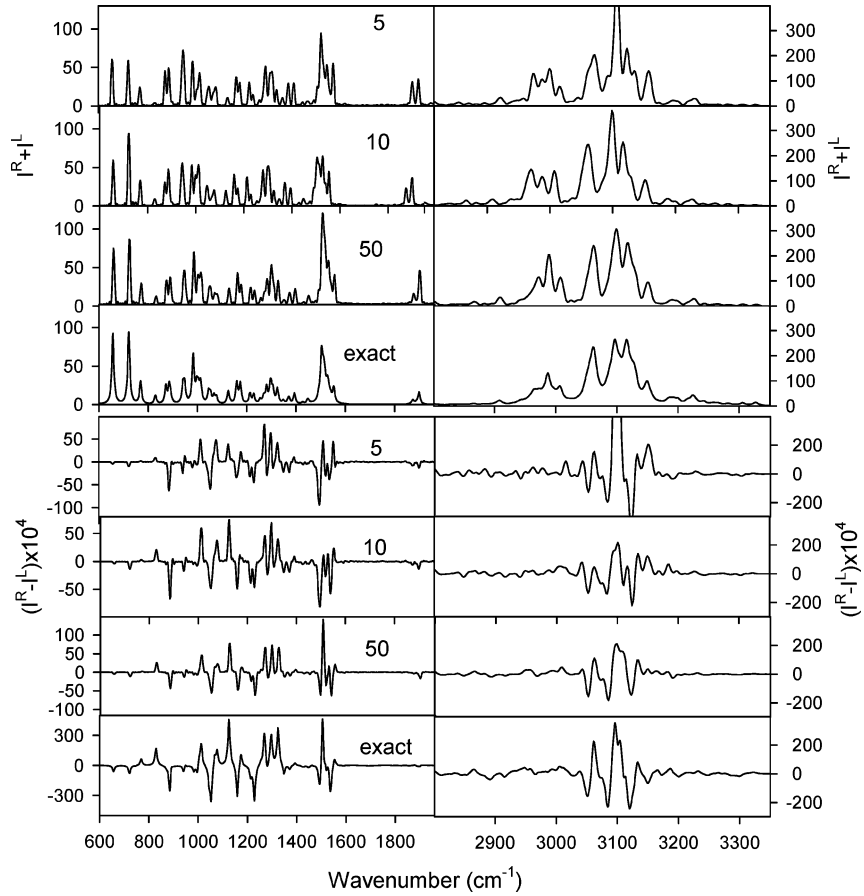

Figure 5. Dependence of the Raman (top) and Raman optical activity (bottom) spectra of fenchone on the number of random vectors used in the propagation.

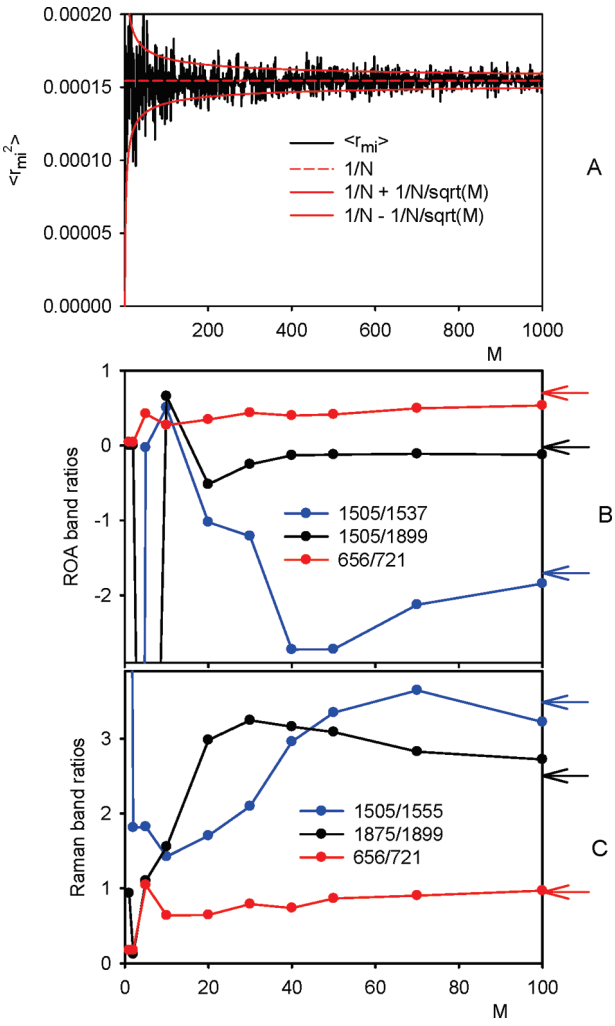

Figure 6. Convergence properties of spectral intensities on the number of random vectors: (A) average, RMS deviation interval[62] ($N^{-1} \pm N^{-1}M^{-1/2}$), and actual values for a random coefficient ($i = 10$) for the fenchone simulation in Figure 5 with $N = 6475$ and ratios of selected (B) ROA and (C) Raman peak intensities. Central peak frequencies are indicated in cm^{-1}; the arrows mark exact values.

coefficient averaging and the root-mean-square deviation that converges as $\sim 1/\sqrt{M}$.[62] Although, as discussed above, we cannot get the actual state probabilities (d_i), from eqs 3−5, it is clear that the intensity will converge in the same manner that this factor does. The possible error proportional to the square root of M converges rather slowly; thus benchmark simulations with large values of M are clearly inefficient. On the other hand, in accord with the observation of the spectral convergence in Figure 5, a reasonable intensity error of ∼10% can be obtained with a limited amount (<100) of the vectors, which is sufficient in many applications of the vibrational spectroscopy.

Actual convergence of the Raman and ROA band ratios (Figure 6, parts B and C) is more complicated due to the band overlaps; however, the trends are clearly given by the basic $1/\sqrt{M}$ dependence for the coefficients. From the figure, we also see that simulations with $M < 20$ should be avoided for ROA, as they may even lead to the wrong signs for some peaks. For the selected examples of three peak pairs in Figure 6, the lowest-energy lone-standing transitions (656/721 cm^{-1}) converge most smoothly.

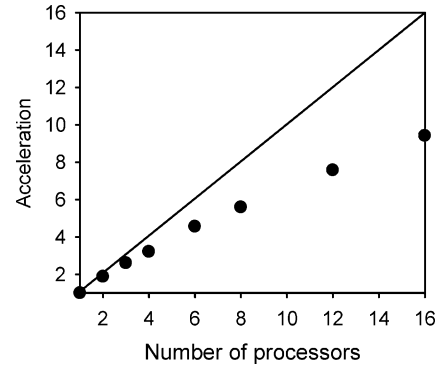

Figure 7. Dependence of the acceleration on the number of processors (fenchone IR spectrum calculation, pgf77-OMP-linux software environment, 4 Intel E7330/2.40 GHz CPUs on Supermicro X7QCE motherboard).

The number of vibrational degrees of freedom associated with the number of atoms does not seem to be important for the convergence properties; the water dimer spectra (not shown) behaved similarly to that of fenchone. However, as the density of vibrational states increases and the peaks became more overlapped in more complex molecules, higher accuracy, and thus presumably a larger number of the starting vectors, will be required for simulations on larger systems.

As observed also for other time-dependent approaches,[29,43] it is difficult to extract information about the individual normal mode contribution to the spectrum. For harmonic potential, this is partially solvable by a specially designed propagation scheme.[63] In anharmonic computations, the concept of normal modes vanishes completely. However, in a majority of practical computations, the harmonic approximation is realistic enough to provide reliable information about the origin of observable transitions.

As the vectors can be propagated independently, the algorithm is amendable to parallelization. Our OMP shared memory implementation (http://openmp.org) did not lead to a perfect scaling (cf. Figure 7); nevertheless, it documents the significant speedups that can easily be achieved on common shared-memory multiprocessor computers. More importantly, the FT algorithm becomes very convenient for larger Hamiltonian dimensions. This is documented in Figure 8, where the diagonalization times needed for the direct and Davidson computations are compared to the FT simulations for variously sized fenchone VCI Hamiltonians. The Davidson method is apparently quite inefficient, and the CPU time rises steeply. The direct diagonalization is very fast for smaller matrices, but the N^3 time and N^2 memory scaling make it inconvenient for larger ones; for $N \sim 6000$, the FT methodology becomes the fastest scheme for the vibrational spectra generation. As pointed out above, slightly longer times are required for more resolved spectra (longer propagation needed) and more accurate spectral intensities (requiring many random vector averaging). Still, the FT method would be the most convenient when the Hamiltonian reaches a certain limit. Additionally, only nonzero Hamiltonian elements need to be stored for FT, unlike for the direct methods.

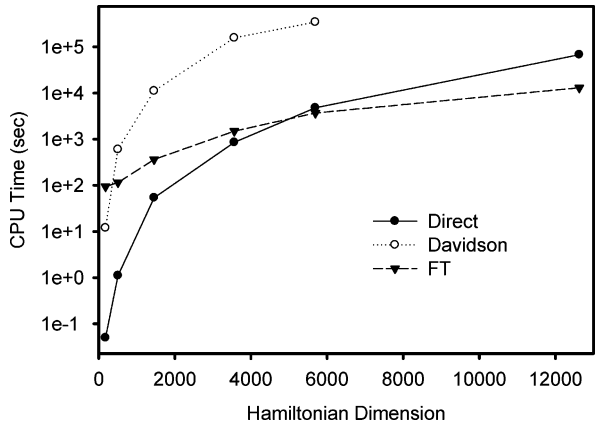

Figure 8. CPU time needed for the fenchone Hamiltonian diagonalization with the direct and Davidson methods, and the FT spectral generation, as a function of the matrix dimension, for one Intel E5530 2.4 GHz processor. The Davidson iteration was limited to wavenumbers below 2000 cm^{-1}; the FT computation was done with 10 000 steps and one random vector only.

V. Conclusions

The proposed computational scheme enabled us to estimate conveniently vibrational spectral profiles based on the VCI Hamiltonian and intensity tensor derivatives. Because the ground state could be calculated by the classical Davidson method, the Fourier transformation with suitably chosen integration steps provided exact transition frequencies. Besides the wave function, electromagnetic tensors (e.g., the electric dipole for infrared absorption) were propagated, which enabled a simultaneous computation of spectral intensities. Only approximate absolute intensities could be simulated; however, propagation of many random vectors and the averaging led to faithful relative band intensities and correct ROA sign patterns, with accuracy sufficient for most molecular structural studies based on the vibrational spectra. For large molecules (large VCI Hamiltonians), the algorithm provided the spectra faster than the classical methods based on the explicit matrix diagonalization.

Acknowledgment. This work was supported by the Grant Agency of the Czech Republic (202/07/0732) and the Grant Agency of the Academy of Sciences (A400550702, M200550902).

References

(1) Kubelka, J.; Bouř, P.; Keiderling, T. A. Quantum Mechanical Calculations of Peptide Vibrational Force Fields and Spectral Intensities. In *Advances in Biomedical Spectroscopy, Biological and Biomedical Infrared Spectroscopy*; Barth, A., Haris, P. I., Eds.; IOS Press: Amsterdam, 2009; Vol. 2, pp 178.

(2) Califano, S. *Vibrational states*; John Wiley & Sons: London, 1976.

(3) Narayanan, U.; Keiderling, T. A. *J. Am. Chem. Soc.* **1983**, *105*, 6406.

(4) Pulay, P. Analytical derivative techniques and the calculation of vibrational spectra. In *Modern electronic structure theory*; Yarkony, D. R., Ed.; World Scientific: Singapore, 1995; Vol. 2, pp 1191.

(5) Cheeseman, J. R.; Frisch, M. J.; Devlin, F. J.; Stephens, P. J. *Chem. Phys. Lett.* **1996**, *252*, 211.

(6) Papoušek, D.; Aliev, M. R. *Molecular Vibrational/Rotational Spectra*; Academia: Prague, 1982.

(7) Bounouar, M.; Scheurer, C. *Chem. Phys.* **2006**, *323*, 87.

(8) Daněček, P.; Kapitán, J.; Baumruk, V.; Bednárová, L.; Kopecký, V., Jr.; Bouř, P. *J. Chem. Phys.* **2007**, *126*, 224513.

(9) Hansen, M. B.; Sparta, M.; Seidler, P.; Toffoli, D.; Christiansen, O. *J. Chem. Theory Comput.* **2010**, *6*, 235.

(10) Andrushchenko, V.; Matějka, P.; Anderson, D. T.; Kaminský, J.; Horníček, J.; Paulson, L. O.; Bouř, P. *J. Phys. Chem. A* **2009**, *113*, 9727.

(11) Fujisaki, H.; Yagi, K.; Hirao, K.; Straub, J. E. *Chem. Phys. Lett.* **2007**, *443*, 6.

(12) Chakraborty, A.; Truhlar, D. G.; Bowman, J. M.; Carter, S. *J. Chem. Phys.* **2004**, *121*, 2071.

(13) Neff, M.; Rauhut, G. *J. Chem. Phys.* **2009**, *131*, 124129.

(14) Bowman, J. M. *J. Chem. Phys.* **1978**, *68*, 608.

(15) Gerber, R. B.; Ratner, M. A. *Chem. Phys. Lett.* **1979**, *68*, 195.

(16) Bounouar, M.; Scheurer, C. *Chem. Phys.* **2008**, *347*, 194.

(17) Norris, L. S.; Ratner, M. A.; Roitberg, A. E.; Gerber, R. B. *J. Chem. Phys.* **1996**, *105*, 11261.

(18) Daněček, P.; Bouř, P. *J. Comput. Chem.* **2007**, *28*, 1617.

(19) Christiansen, O. *J. Chem. Phys.* **2004**, *120*, 2149.

(20) Christiansen, O.; Luis, J. M. *Int. J. Quantum Chem.* **2005**, *104*, 667.

(21) Schleyer, P. R.; Allinger, N. L.; Clark, T.; Gasteiger, J.; Kollman, P. A.; Schaefer, H. F., III; Schreiner, P. R. *The Encyclopedia of Computational Chemistry*; John Wiley & Sons: Chichester, U.K., 1998.

(22) Grotendorst, J. *Modern methods and algorithms of quantum chemistry*; John von Neumann Institute for Computing: Julich, Germany, 2000; Vol. 1.

(23) Press, W. H.; Teukolsky, S. A.; Vetteling, W. T.; Flannery, B. P. *Numerical Recipes in Fortran*, 2nd ed.; Cambridge University Press: New York, 1992.

(24) Kaledin, A. L.; Kaledin, M.; Bowman, J. M. *J. Chem. Theory Comput.* **2006**, *2*, 166.

(25) Davidson, E. R. *J. Comput. Phys.* **1975**, *17*, 87.

(26) Martins, J. L.; Cohen, M. L. *Phys. Rev. B* **1988**, *37*, 6134.

(27) Mitin, A. V. *J. Comput. Chem.* **1994**, *15*, 747.

(28) vanderVorst, H. A. *Iterative Krylov Methods for Large Linear Systems*; Cambridge University Press: Cambridge, U. K., 2003.

(29) Horníček, J.; Kaprálová, P.; Bouř, P. *J. Chem. Phys.* **2007**, *127*, 084502.

(30) Kubelka, J.; Bouř, P. *J. Chem. Theory Comput.* **2009**, *5*, 200.

(31) Gordon, R. G. *J. Chem. Phys.* **1965**, *42*, 3658.

(32) Noid, D. W.; Koszykowski, M. L.; Marcus, R. A. *J. Chem. Phys.* **1977**, *67*, 404.

(33) Abbate, S.; Longhi, G.; Kwon, K.; Moscowitz, A. *J. Chem. Phys.* **1998**, *108*, 50.

(34) Kim, H.; Rossky, P. J. *J. Chem. Phys.* **2006**, *125*, 074107.

(35) Kinnaman, C. S.; Cremeens, M. E.; Romesberg, F. E.; Corcelli, S. A. *J. Am. Chem. Soc.* **2006**, *128*, 13334.

(36) Hahn, S.; Lee, H.; Cho, M. *J. Chem. Phys.* **2004**, *121*, 1849.

(37) Mankoo, P. K.; Keyes, T. *J. Chem. Phys.* **2006**, *124*, 204503.

(38) Lee, K. K.; Hahn, S.; Oh, K. I.; Choi, J. S.; Joo, C.; Lee, H.; Han, H.; Cho, M. *J. Phys. Chem. B* **2006**, *110*, 18834.

(39) Torii, H. *J. Phys. Chem. A* **2006**, *110*, 9469.

(40) Gnanakaran, S.; Hochstrasser, R. M. *J. Am. Chem. Soc.* **2001**, *123*, 12886.

(41) Loparo, J. J.; Roberts, S. T.; Tokmakoff, A. *J. Chem. Phys.* **2006**, *125*, 194521.

(42) Krummel, A. T.; Zanni, M. T. *J. Phys. Chem. B* **2006**, *110*, 24720.

(43) Silva, A. J. R.; Pang, J. W.; Carter, E. A.; Neuhauser, D. *J. Phys. Chem. A* **1997**, *102*, 881.

(44) Liang, Y.; Miranda, C. R.; Scandolo, S. *J. Chem. Phys.* **2006**, *125*, 194524.

(45) Yang, S.; Cho, M. *J. Phys. Chem. B* **2007**, *111*, 605.

(46) Gorbunov, R. D.; Nguyen, P. H.; Kobus, M.; Stock, G. *J. Chem. Phys.* **2007**, *126*, 054509.

(47) Yamauchi, Y.; Nakai, H. *J. Chem. Phys.* **2004**, *121*, 11098.

(48) Putrino, A.; Parrinello, M. *Phys. Rev. Lett.* **2002**, *88*, 176401.

(49) Seibt, J.; Engel, V. *J. Chem. Phys.* **2007**, *126*, 074110.

(50) Meyer, H. D.; Le Quere, F.; Leonard, C.; Gatti, F. *Chem. Phys.* **2006**, *329*, 179.

(51) Murray, C. W.; Racine, S. C.; Davidson, E. R. *J. Comput. Chem.* **1992**, *103*, 382.

(52) Charney, E. *The Molecular Basis of Optical Activity*; Wiley-Interscience: New York, 1979.

(53) Bouř, P. *S4*; Academy of Sciences: Prague, 1994−2010.

(54) Frisch, M. J.; Trucks, G. W.; Schlegel, H. B.; Scuseria, G. E.; Robb, M. A.; Cheeseman, J. R.; Montgomery, J. A., Jr.; Vreven, T.; Kudin, K. N.; Burant, J. C.; Millam, J. M.; Iyengar, S. S.; Tomasi, J.; Barone, V.; Mennucci, B.; Cossi, M.; Scalmani, G.; Rega, N.; Petersson, G. A.; Nakatsuji, H.; Hada, M.; Ehara, M.; Toyota, K.; Fukuda, R.; Hasegawa, J.; Ishida, M.; Nakajima, T.; Honda, Y.; Kitao, O.; Nakai, H.; Klene, M.; Li, X.; Knox, J. E.; Hratchian, H. P.; Cross, J. B.; Bakken, V.; Adamo, C.; Jaramillo, J.; Gomperts, R.; Stratmann, R. E.; Yazyev, O.; Austin, A. J.; Cammi, R.; Pomelli, C.; Ochterski, J. W.; Ayala, P. Y.; Morokuma, K.; Voth, G. A.; Salvador, P.; Dannenberg, J. J.; Zakrzewski, V. G.; Dapprich, S.; Daniels, A. D.; Strain, M. C.; Farkas, O.; Malick, D. K.; Rabuck, A. D.; Raghavachari, K.; Foresman, J. B.; Ortiz, J. V.; Cui, Q.; Baboul, A. G.; Clifford, S.; Cioslowski, J.; Stefanov, B. B.; Liu, G.; Liashenko, A.; Piskorz, P.; Komaromi, I.; Martin, R. L.; Fox, D. J.; Keith, T.; Al-Laham, M. A.; Peng, C. Y.; Nanayakkara, A.; Challacombe, M.; Gill, P. M. W.; Johnson, B.; Chen, W.; Wong, M. W.; Gonzalez, C.; Pople, J. A. *Gaussian 03*, Revision C.02; Gaussian, Inc.: Wallingford, CT, 2004.

(55) Barron, L. D. *Molecular Light Scattering and Optical Activity*; Cambridge University Press: Cambridge, U. K., 2004.

(56) Polavarapu, P. L. *Vibrational Spectra and Structure* **1984**, *13*, 103.

(57) Becke, A. D. *J. Chem. Phys.* **1993**, *98*, 5648.

(58) Johnson, K. *Numerical Methods in Chemistry*; Marcel Dekker, Inc.: New York, 1980; Vol. 7.

(59) Keiderling, T. A.; Kubelka, J.; Hilario, J. Vibrational circular dichroism of biopolymers. Summary of methods and applications. In *Vibrational spectroscopy of polymers and biological systems*; Braiman, M., Gregoriou, V., Eds.; CRC Press: Boca Raton, FL, 2006; pp 253.

(60) Krimm, S. Vibrational spectroscopy of polypeptides. In *Modern Polymer Spectroscopy*; Zerbi, G., Ed.; Wiley-VCH: New York, 1999; pp 239.

(61) Longhi, G.; Abbate, S.; Gangemi, R.; Giorgio, E.; Rosini, C. *J. Phys. Chem. A* **2006**, *110*, 4958.

(62) Everitt, B. S. *The Cambridge Dictionary of Statistics*; Cambridge University Press: Cambridge, U. K., 2002; p 410.

(63) Martines, M.; Gaigeot, M. P.; Borgis, D.; Vuilleumier, R. *J. Chem. Phys.* **2006**, *125*, 144106.

CT100150F